Chapter 7

Impact of Solar Forcing on Thermospheric Densities and Spacecraft Orbits from CHAMP and GRACE

Jiuhou Lei, Guangming Chen, Jiyao Xu and Xiankang Dou

Additional information is available at the end of the chapter

http://dx.doi.org/10.5772/56599

1. Introduction

The thermosphere is the outer gaseous shell of a planet's atmosphere that exchanges energy with the space plasma environment. The energy deposition of solar irradiation and magnetospheric inputs into the upper atmosphere can change the thermospheric density significantly. From a practical standpoint, unanticipated changes in the density of the thermosphere cause satellites to deviate from their anticipated paths, or ephemerides. Many studies have been pursued to investigate the variations of thermospheric densities caused by solar forcing, which includes solar irradiation and magnetospheric energy deposition [1-12]. However, the quantitative examination of the impact of thermospheric density changes associated with solar forcing on satellite orbits is rare, given that the simultaneous measurements of thermospheric density and precise tracking data of satellite are sparse.

Recently, we utilized the measurements obtained from the Challenging Minisatellite Payload (CHAMP) and the Gravity Recovery and Climate Experiment (GRACE) satellites to study the impact of solar irradiation and solar wind forcing on thermospheric density and satellite orbits as well [e.g., 13-14]. The CHAMP and GRACE satellites provided simultaneous observations for both thermospheric density and satellite orbit data. The CHAMP satellite was launched in July 2000 at 450 km altitude in a near-circular orbit with an inclination of 87.3°. Meanwhile, two identical satellites GRACE-A and GRACE-B were launched in March 2002 at approximately 500 km altitude, in near-circular 89.5° inclination orbits with GRACE-B following approximately 220 km behind GRACE-A. Then the mass densities are obtained from CHAMP and GRACE accelerometer measurements using standard methods [15]. Note that only GRACE-A data are used for this study, given that the mass densities from GRACE-A and GRACE-B show very similar variations. On the other hand, the GPS receiver aboard CHAMP

and GRACE satellites can provide precise tracking data of the spacecraft orbits [16]. The change of satellite altitude is caused by thermospheric drag that is proportional to thermospheric density ρ [13]:

$$\frac{dr}{dt} = -C_D \frac{A}{m} \sqrt{GMr}\,\rho \tag{1}$$

where r is the mean radius between the satellite and the Earth, C_D is the drag coefficient, m is the satellite mass, M is the mass of the Earth, G is the gravitation constant and A is the surface area of the satellite. Therefore, these simultaneous observations from CHAMP and GRACE for both thermospheric density and orbit tracking data at a high temporal resolution provide a good opportunity to explore the impact of thermospheric density on spacecraft orbits in a quantitative way.

2. Solar activity dependence of thermospheric density and satellite orbit

Figure 1 shows the temporal variations of daily mean thermospheric density, decay rate of satellite orbit per day of CHAMP and the corresponding NOAA hemispheric power (HP) from 2001 to 2006. It is clear that the variations of thermospheric density are well correlated with those of satellite orbit decay rate. Both thermospheric density and orbit decay rate show evident seasonal and solar cycle variations. The seasonal variation of thermospheric density and the resultant change in the orbit decay rate are explained by the thermospheirc spoon effect [17] and the seasonal variation of the lower atmospheric forcing associated with eddy mixing in the mesopause region [18]. In addition, the long term trend of thermospheric density and orbit decay rate is mainly driven by the corresponding changes of solar forcing [19], which is indicated by the F10.7 proxy and auroral hemispheric power HP [20].

There is a 27-day period variation of the densities, which is mainly caused by the periodic oscillation of solar radiation induced by solar rotation [3, 13]. The orbit decay rate of CHAMP, which is caused by the atmospheric drag, has the similar oscillations with the densities. Figure 2 gives the results for solar EUV flux, thermospheric densities observed by CHAMP and GRACE and orbital radiuses of the two satellites after a band-pass filter. The band-pass filter was centered at the period of 27 days, with half-power points at 22 and 32 days. It is obvious that both thermospheric densities and satellite orbital radiuses had a strong response to the 27 day oscillation in solar radiation. High correlations were found for the oscillations between thermospheric density, mean radius of the satellite orbit and EUV, especially when a strong quasi-27 day periodicity was present.

As seen in Figure 2, the amplitudes of the oscillations in thermosperic density and mean radius of satellite orbit of CHAMP were larger than those of GRACE. Given that the altitude of the GRACE was about 100 km higher than that of the CHAMP, the effect of thermospheric drag was weaker at the GRACE altitude. The oscillation of mean radius of the satellite orbit per revolution was about 0.1 km for CHAMP, while it was about 0.05 km for GRACE during the

http://dx.doi.org/10.5772/56599

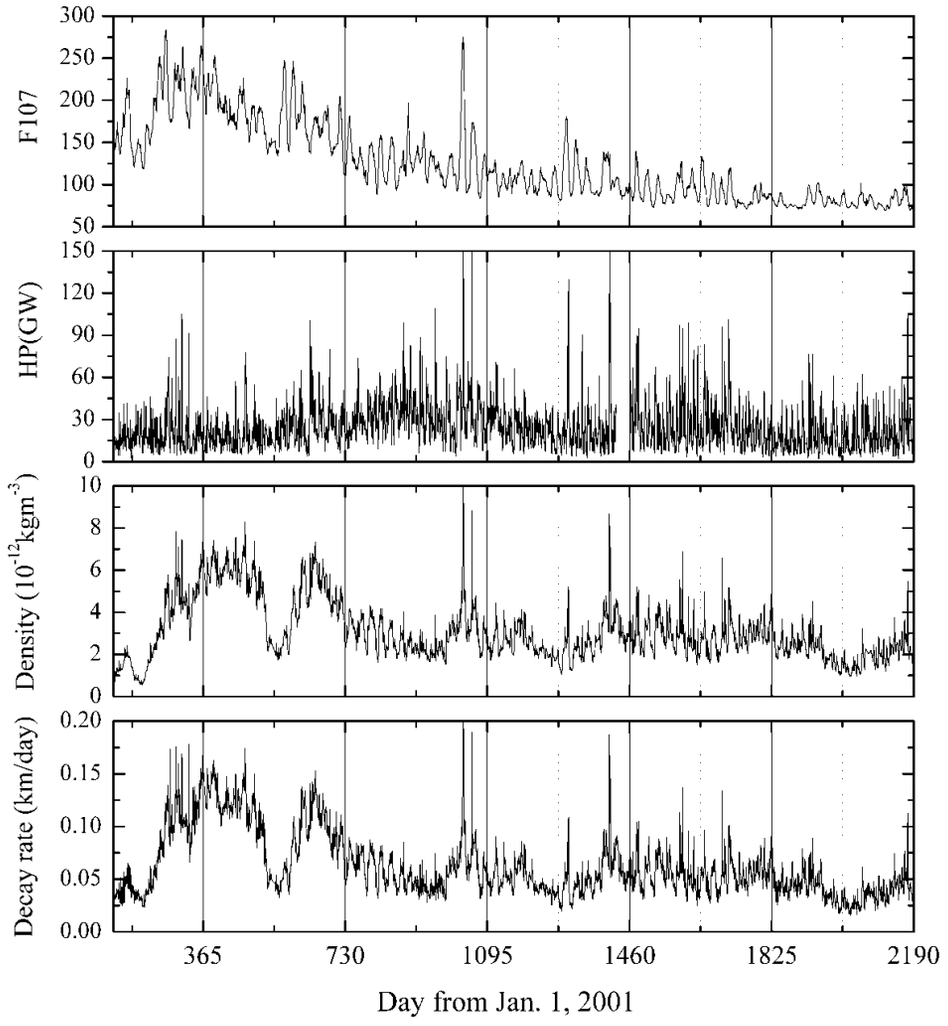

Figure 1. Variations of the F10.7, daily averaged auroral hemispheric power (HP), thermospheric density, and decay rate of the satellite orbit per day of CHAMP during 2001-2006. The day number is accounted from January 1, 2001.

first half of 2003. As the solar activity declines, the oscillations in thermospehric density and satellite orbit tend to decrease, for example in 2005.

Note that multi-day oscillations at the periods of 7 and 9 days were observed in the thermospheric densities [8-10], which are caused by the solar wind high-speed streams and the associated recurrent geomagnetic activity. The effect of the multi-day oscillations in thermospheric density is also imbedded in the satellite orbital radiuses [13]. Besides the periodic oscillations, sudden enhancements of thermospheric density and decay rate of satellite orbit, which are caused by the geomagnetic storms, are also seen simultaneously in Figure 1. For example, the enhancements during those storms in October, November in 2003 and November in 2004 are especially significant due to the large magnetospheric energy deposition. The values of the thermospheric density and orbit decay rate in the October 2003 Halloween storm reach their maximum, which are larger than 1×10^{-11} kg m^{-3} and 0.22 km/day, respectively. In

the next section, we will give more details about the variations of thermosphere density and satellite orbits during the storm events.

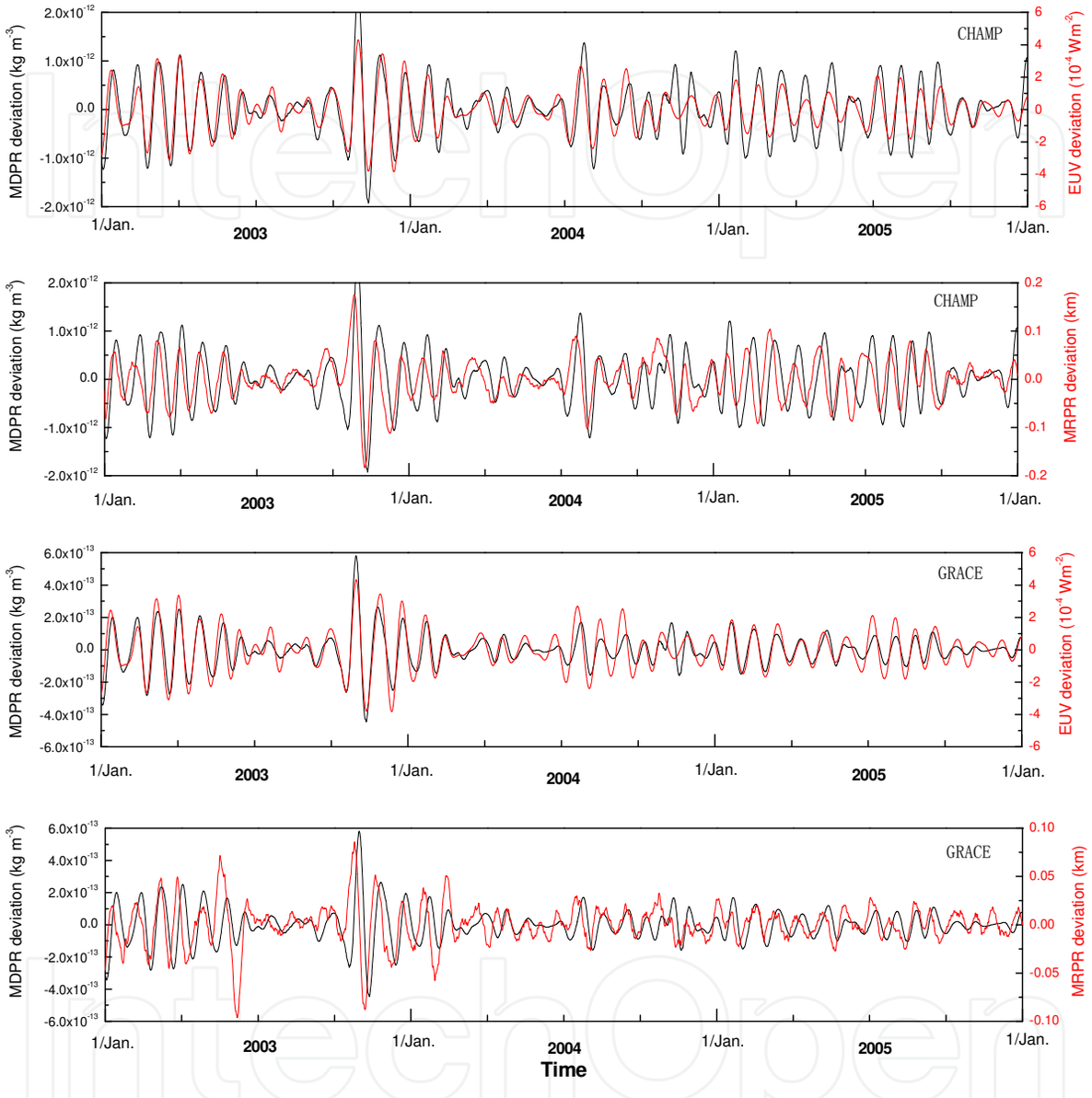

Figure 2. Band-pass filtered time series of EUV flux, mean thermospheric density per revolution (MDPR), and mean radius of satellite orbit per revolution (MRPR). From top to bottom: first panel, EUV flux and CHAMP MDPR; second panel, CHAMP MDPR and MRPR; third panel, EUV flux and GRACE MDPR; fourth panel, GRACE MDPR and MRPR. See [13].

3. Orbital variations induced by CME and CIR storms

There are significant differences between geomagnetic storms driven by coronal mass ejections (CME) and by corotating interaction regions (CIRs)/high speed solar wind streams [21, 12].

http://dx.doi.org/10.5772/56599

Usually, the strength of magnetospheric convection electric field of a CME-storm is stronger than that of a CIR-storm [22]. However, the duration of a CIR-storm is oftern much longer than that of CME [23, 14]. Although the rate of solar wind energy input into the magnetosphere of CIR is far less than that during coronal mass ejection (CME) magnetic storm intervals, the energy input over longer durations of time, e.g., several days or even longer, can be greater during high speed stream intervals [e.g., 24-26]. In this section, thermospheric densities and the orbit parameters from CHAMP are used to address the responses of satellite orbital altitudes to geomagnetic activity caused by CME and CIR storms.

Figure 3 shows, from top to bottom, the $F_{10.7}$ index, IMF B_z, solar wind density and velocity, *Dst*, *ap* and *AE* indices, auroral hemispheric power (HP) and thermospheric densities observed by CHAMP, satellite orbit decay rate and total orbit decay on days 323-326, 2003. The detail for the calculation of orbit decay rate can be found in Chen et al. [14]. The proxy F10.7 varied around 170 during this period, indicating high solar activity condition for this case. A geomagnetic storm occurred at 0728 UT on day 324, which is indicated by vertical line in Figure 3. This storm had a large IMF Bz southward component of about -46 nT during the main phase of the event. After the start of the storm, solar wind speed underwent a gradual increase from ~500 km/s to 700 km/s on day 324. The storm had a minimum Dst of -422 nT, which made it a strongest storm in the 23rd solar cycle using the *Loewe and Prölss* classification [27]. The maximum values of *ap* and *AE* reached 300 nT and 1698 nT, respectively. The auroral hemispheric power also increased significantly with a maximum of ~300 GW, indicating enhanced particle precipitation energy deposited into the ionosphere/thermosphere. At about 0100 UT on day 325, Bz turned northward and AE and HP recovered gradually to their pre-storm values. In response to geomagnetic activity and energy deposition, thermospheric density increased significantly. The averaged thermospheric densities reached a maximum of ~1.3×10^{-11} kg•m^{-3} at ~1900 UT on day 324 from its pre-storm value of ~3×10^{-12} kg•m^{-3}. Similar to the thermospheric density, the satellite orbit decay rate also reached a maximum of 279 m/day at ~2100 UT on day 324. Both thermospheric density and orbital decay rate recovered to their pre-storm values around the end of day 325.

Another geomagnetic storm (Storm 2) we are focusing on was caused by high speed solar wind streams and the resultant CIR that hit the Earth at about 1900 UT on day 258. As shown in Figure 4, this storm had a southward Bz excursion with a maximum amplitude of about 7 nT. The solar wind velocity increased from ~400 km/s to 800 km/s on day 261. The minimum of Dst for this storm was -57 nT on day 260, which denotes a moderate geomagnetic storm [27]. The maximum values of *ap*, AE index and HP reached 132 nT, 1228 nT and 125 GW, respectively, which are much smaller than those in the CME in Figure 3. Unlike the CME storm as shown previously (Storm 1), in which IMF Bz turned northward and AE, HP as well as thermospheric density, recovered rapidly after 0200 UT on day 325, this CIR storm had an oscillating IMF Bz that lasted for several days with high AE and HP values. Thermospheric density also stayed an elevated level till day 270. This is related to Alfvenic fluctuations in IMF and high speed streams that followed the CIR interval as discussed by *Tsurutani and Gonzalez* [23] and *Tsurutani et al.* [25]. The thermospheric density and orbital decay rate increased rapidly and reached the values of ~3.2×10^{-12} kg•m^{-3} and 68 m/day from their pre-storm values

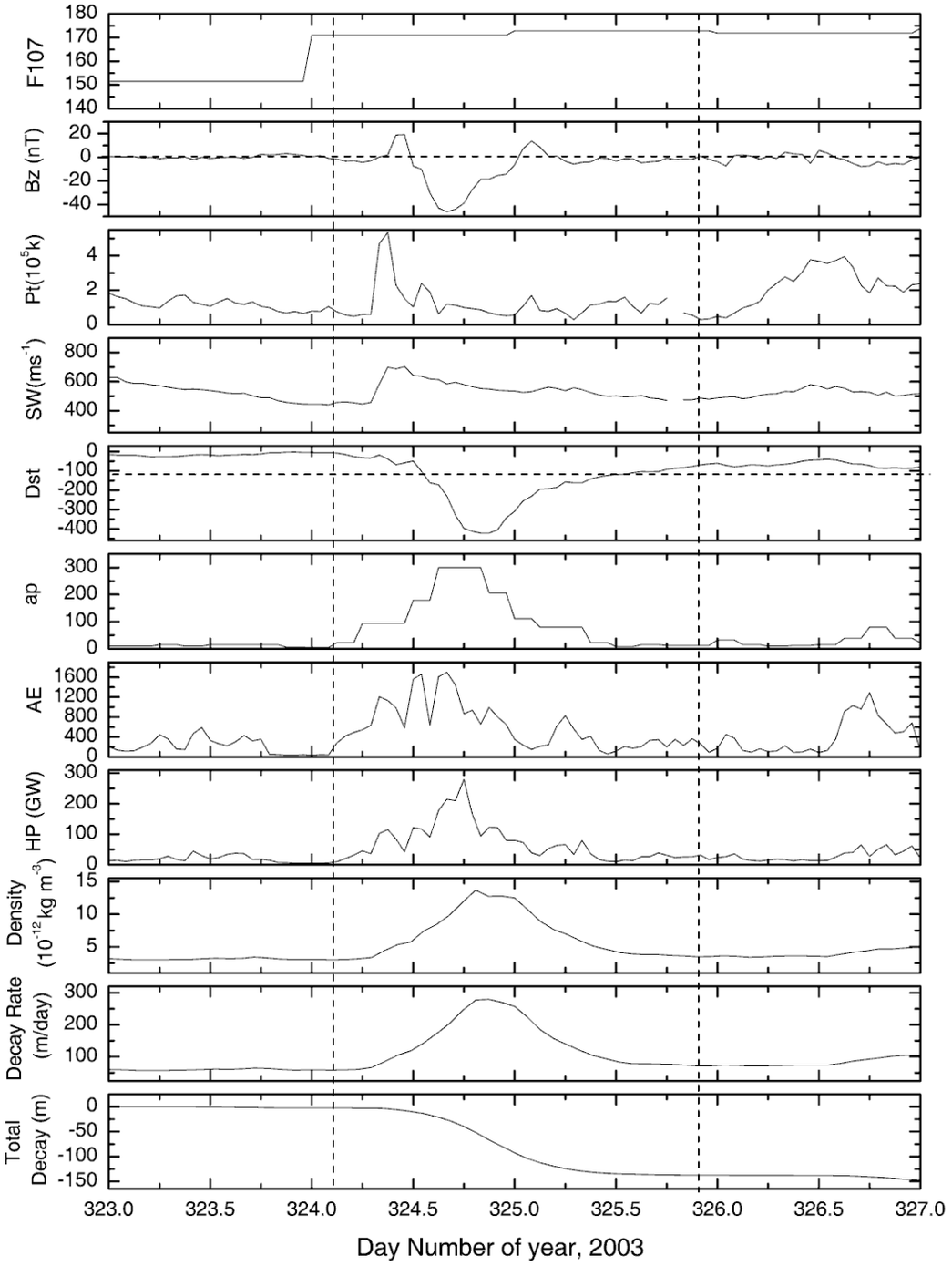

Figure 3. Variations of F10.7, hourly averaged Bz (nT), solar wind temperature (K), solar wind speed (km/s), Dst, ap, AE (nT), auroral hemispheric power (HP) and thermospheric density, CHAMP orbit decay rate and geomagnetic activities induced total orbit decays during November 19-22, 2003 (day 323-326, 2003). The dashed lines show the start and the end of the storm.

http://dx.doi.org/10.5772/56599

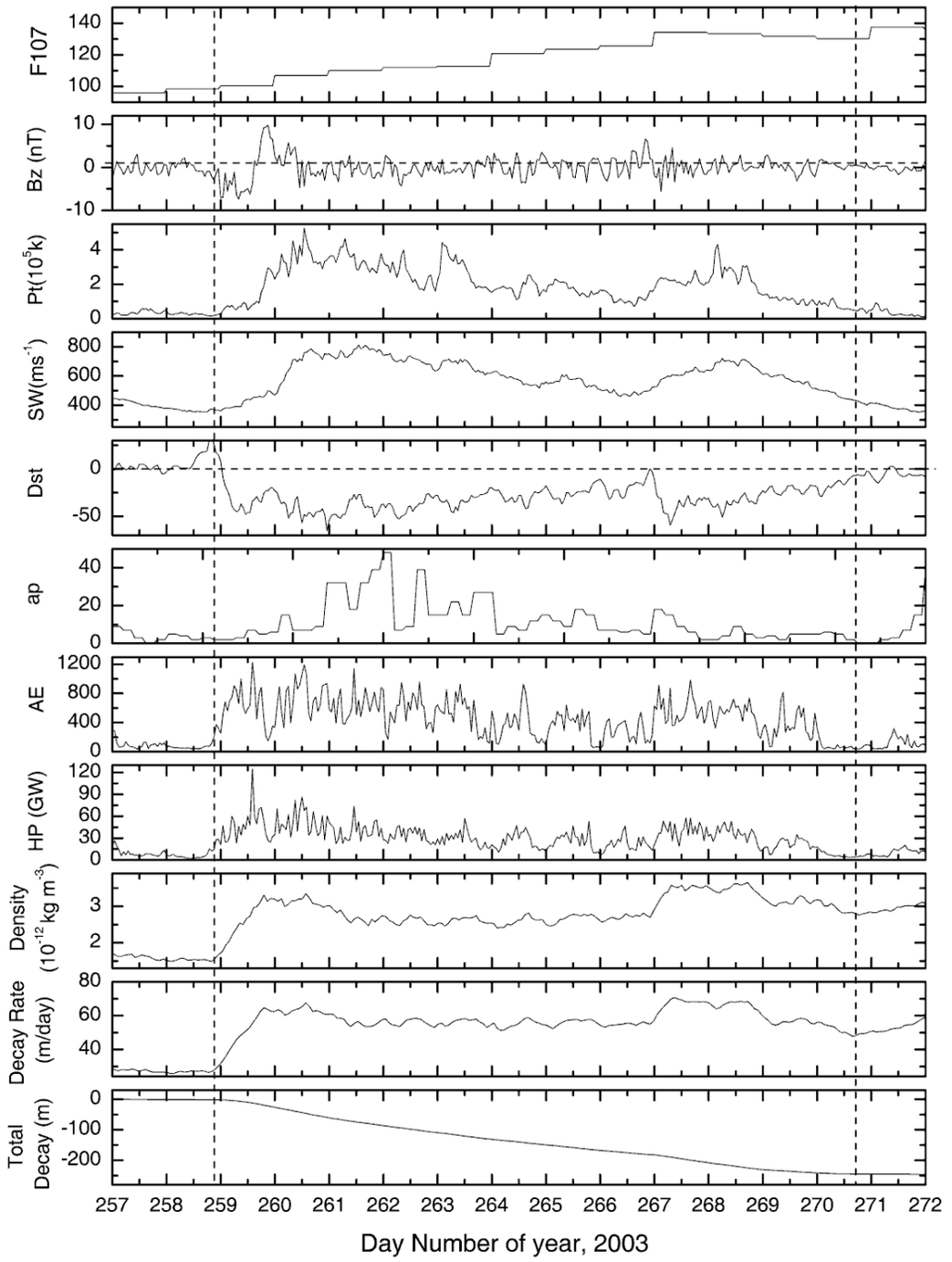

Figure 4. Same as Figure 3, but for the storm event during September 14-28, 2003 (day 257-271, 2003)

of ~1.5×10^{-12} kg•m^{-3} and 27 m/day, respectively. As indicated by the vertical lines in Figures 3-4, the duration of Storm 1 was 1.59 days, and that of Storm 2 was 11.98 days. Thus Storm 2

persisted for a much longer period of time, which consequently produced sustained perturbations to thermospheric densities and satellite orbits.

The total changes of orbit mean semi-major axis induced by these two storms are then calculated by subtracting the observed variations in the semi-major axis from presumed semi-major axis variations as a result of the drag by the quiet-time, background thermosphere. For Strom 1, the storm-induced total variation of the semi-major axis was 130 m. For Storm 2, the corresponding variation was 242 m, about a factor of 1.8 of Storm 1. Storm 1 is evidently stronger, with deeper Dst minimum, stronger auroral activity, greater density changes and larger orbital decay rates than Storm 2; however, it lasted a much shorter time. Thus, the cumulative effect on thermospheric density and satellite orbit is less than that of Storm 2. As a result, the total orbit decay caused by a strong CIR-storm can be larger than that by a severe CME-storm. However, further comprehensive data analysis is required to explore the impact of CME and CIR storms on the satellite orbit changes in a statistical way.

4. Summary

Thermosphere densities can be inferred from the CHAMP and GRACE accelerometer measurements with much higher temporal and spatial resolution than previous satellite drag data in the upper thermosphere. Thus, the CHAMP and GRACE observations provide a unique opportunity to investigate the impact of thermospheric density changes associated with the solar forcing on satellite orbits. It is found that both thermospheric densities and the resultant satellite orbit change vary significantly with solar activity. The oscillation amplitude of mean radius of the satellite orbit per revolution, which is associated with the periodic oscillation of solar radiation induced by solar rotation, can be as large as 0.1 km for the CHAMP, while it was about 0.05 km for the GRACE.

The CHAMP and GRACE data have elucidated the thermosphere response to geomagnetic storms in unprecedented detail. However, the effectiveness of the CME- and CIR-type storms on satellite orbits is not well understood, albeit the differences between geomagnetic storms driven by CME and by CIRs/high speed solar wind streams were recognized from the interplanetary/solar wind structure viewpoint. Our case studies showed that the severe CME storm caused larger thermosphere density disturbance and the resultant orbital decay rates during its main phase, whereas it lasted a much shorter duration to compare with the CIR/high speed stream event. However, the CIR storm can persist for many days and then produce sustained perturbations to thermospheric densities and satellite orbits. As demonstrated in our calculation, total variation of the semi-major axis was 242 m for the CIR storm during September 15-27, 2003 in contrast to 130 m for the CME superstorm event during November 20-21, 2003. Therefore, the CIR storm can also cause significant impact on the thermospheric density and the resultant satellite orbit change, given that it has long duration and occurs frequently during the declining phase of a solar cycle and solar minimum.

Acknowledgements

This work is partly supported by the National Natural Science Foundation of China (41174139, 41274157, 41104098, 41004062), the Project of Chinese Academy of Sciences (KZZD-EW-01), China Postdoctoral Science foundation (20100481450, 201104799) and the Open Research Foundation of Science and Technology on Aerospace Flight Dynamics Laboratory (2012afdl1027). We also acknowledge the CEDAR data based at the National Center for Atmospheric Research (NCAR) for providing the auroral hemispheric power data used in this study. The ap and F10.7 indices were downloaded from NGDC database, and the ACE solar wind data were obtained from the GSFC/SPDF OMNIWeb interface at http://omniweb.gsfc.nasa.gov.

Author details

Jiuhou Lei[1*], Guangming Chen[2], Jiyao Xu[2] and Xiankang Dou[1]

*Address all correspondence to: leijh@ustc.edu.cn

1 CAS Key Laboratory of Geospace Environment, University of Science and Technology of China, Hefei, Anhui, China

2 State Key Laboratory for Space Weather, Center for Space Sciences and Applied Research, Chinese Academy of Sciences, Beijing, China

References

[1] Eastes, R., S. Bailey, B. Bowman, F. Marcos, J. Wise, and T. Woods (2004), The correspondence between thermospheric neutral densities and broadband measurements of the total solar soft X-ray flux, Geophys. Res. Lett., 31, L19804, doi: 10.1029/2004GL020801.

[2] Forbes, J. M., G. Lu, L. S. Bruinsma, R. S. Nerem, and X. Zhang (2005), Thermosphere density variations due to the 15–24 April 2002 solar events from CHAMP/STAR accelerometer measurements, J. Geophys. Res., 110, A12S27, doi:10.1029/2004JA010856.

[3] Forbes, J. M., S. Bruinsma, and F. G. Lemoine (2006), Solar rotation effects in the thermospheres of Mars and Earth, Science, 312, 1366– 1368.

[4] Sutton, E. K., J. M. Forbes, and R. S. Nerem (2005), Global thermospheric neutral density and wind response to the severe 2003 geomagnetic storms from CHAMP accelerometer data, J. Geophys. Res., 110, A09S40, doi:10.1029/2004JA010985.

[5] Liu, H., and H. Lühr (2005), Strong disturbance of the upper thermospheric density due to magnetic storms: CHAMP observations, J. Geophys. Res., 110, A09S29, doi: 10.1029/2004JA010908.

[6] Bruinsma, S. L., J. M. Forbes, R. S. Nerem, and X. Zhang (2006), Thermosphere density response to the 20–21 November 2003 solar and geomagnetic storm from CHAMP and GRACE accelerometer data, J. Geophys. Res., 111, A06303, doi: 10.1029/2005JA011284.

[7] Guo, J., W. Wan, J. M. Forbes, E. Sutton, R. S. Nerem, T. N. Woods, S. Bruinsma, and L. Liu (2007), Effects of solar variability on thermosphere density from CHAMP accelerometer data, J. Geophys. Res., 112, A10308, doi:10.1029/2007JA012409.

[8] Thayer, J. P., J. Lei, J. M. Forbes, E. K. Sutton, and R. S. Nerem (2008), Thermospheric density oscillations due to periodic solar wind high-speed streams, J. Geophys. Res., 113, A06307, doi:10.1029/2008JA013190.

[9] Lei, J., J. P. Thayer, J. M. Forbes, E. K. Sutton, and R. S. Nerem (2008), Rotating solar coronal holes and periodic modulation of the upper atmosphere, Geophys. Res. Lett., 35, L10109, doi:10.1029/2008GL033875.

[10] Lei, J., J. P. Thayer, J. M. Forbes, E. K. Sutton, R. S. Nerem, M. Temmer, and A. M. Veronig (2008), Global thermospheric density variations caused by high-speed solar wind streams during the declining phase of solar cycle 23, J. Geophys. Res., 113, A11303, doi:10.1029/2008JA013433.

[11] Lei, J., J. P. Thayer, G. Lu, A. G. Burns, W. Wang, E. K. Sutton, and B. A. Emery (2011), Rapid recovery of thermosphere density during the October 2003 geomagnetic storms, J. Geophys. Res., 116, A03306, doi:10.1029/2010JA016164.

[12] Lei, J., J. P. Thayer, W. Wang, and R. L. McPherron (2011), Impact of CIR storms on thermosphere density variability during the solar minimum of 2008, Sol. Phys., 274, 427-437, doi:10.1007/s11207-010-9563-y.

[13] Xu, J., W. Wang, J. Lei, E. K. Sutton, and G. Chen (2011), The effect of periodic variations of thermospheric density on CHAMP and GRACE orbits, J. Geophys. Res., 116, A02315, doi:10.1029/2010JA015995.

[14] Chen, G., J. Xu, W. Wang, J. Lei, and A. G. Burns (2012), A comparison of the effects of CIR- and CME-induced geomagnetic activity on thermospheric densities and spacecraft orbits: Case studies, J. Geophys. Res., 117, A08315, doi: 10.1029/2012JA017782.

[15] Sutton, E. K., R. S. Nerem, and J. M. Forbes (2007), Density and winds in the thermosphere deduced from accelerometer data, J. Spacecr. Rockets, 44, 1210–1219, doi: 10.2514/1.28641.

[16] Reigber, C., H. Lühr, and P. Schwintzer (2002). CHAMP mission status. Adv. Space Res., 30 (2), 129–134.

[17] Fuller-Rowell, T. J. (1998), The ''thermospheric spoon'': A mechanism for the semiannual density variation, J. Geophys. Res., 103, 3951– 3956.

[18] Qian, L., S. C. Solomon, and T. J. Kane (2009), Seasonal variation of thermospheric density and composition, J. Geophys. Res., 114, A01312, doi: 10.1029/2008JA013643.

[19] Knipp, D. J., W. K. Tobiska, B. A. Emery (2004), Direct and indirect thermospheric heating sources for solar cycles 21-23, Sol. Phys., 224, 495-505.

[20] Emery, B. A., I. G. Richardson, D. S. Evans, R. J. Rich, and W. Xu (2009), Solar wind structure sources and periodicities of global electron hemispheric power over three solar cycles, J. Atmos. Sol. Terr. Phys., 71, 1157–1175, doi:10.1016/j.jastp.2008.08.005.

[21] Borovsky, J. E., and M. H. Denton (2006), Differences between CME-driven storms and CIR-driven storms, J. Geophys. Res., 111, A07S08, doi:10.1029/2005JA011447.

[22] Denton, M. H., J. E. Borovsky, R. M. Skoug, M. F. Thomsen, B. Lavraud, M. G. Henderson, R. L. McPherron, J. C. Zhang, and M. W. Liemohn (2006), Geomagnetic storms driven by ICME- and CIR-dominated solar wind, J. Geophys. Res., 111, A07S07, doi:10.1029/2005JA011436.

[23] Tsurutani, B. T., and W. D. Gonzalez (1987), The cause of high-intensity long-duration continuous AE activity (HILDCAAs): Interplanetary Alfven wave trains, Planet. Space Sci., 35, 405-412.

[24] Tsurutani, B. T., W. D. Gonzalez, A. L. C. Gonzalez, F. Tang, J. K. Arballo, and M. Okada (1995), Interplanetary origin of geomagnetic activity in the declining phase of the solar cycle, J. Geophys. Res., 100(A11), 21,717– 21,733.

[25] Tsurutani, B. T., et al. (2006), Corotating solar wind streams and recurrent geomagnetic activity: A review, J. Geophys. Res., 111, A07S01, doi:10.1029/2005JA011273.

[26] Kozyra, J. U., et al. (2006), Response of the upper/middle atmosphere to coronal holes and powerful high-speed solar wind streams in 2003, in Recurrent Magnetic Storms: Corotating Solar Wind Streams, Geophys. Monogr. Ser., vol. 167, edited by B. T. Tsurutani et al., pp. 319–340, AGU, Washington, D. C.

[27] Loewe, C. A., and G. W. Pröss (1997), Classification and mean behavior of magnetic storms, J. Geophys. Res., 102 (A7), 14209-14214.

IntechOpen